===== **METALS** =====

Effect of Annealing in a Ferromagnetic State on the Structure of an Fe−18 at % Ga Alloy

Yu. P. Chernenkov[a], N. V. Ershov[b], *, and V. A. Lukshina[b, c]**

[a] *Petersburg Nuclear Physics Institute, National Research Center "Kurchatov Institute,"*
Gatchina, Leningradskaya oblast, 188300 Russia
[b] *Institute of Metal Physics, Ural Branch, Russian Academy of Sciences, Yekaterinburg, 620108 Russia*
[c] *Ural Federal University Named after the First President of Russia B.N. Yeltsin, Yekaterinburg, 620002 Russia*
***e-mail: nershov@imp.uran.ru**
Received June 26, 2018

Abstract—The atomic structure of the iron−gallium alloy containing 18 at % Ga has been studied by X-ray diffraction. The samples were annealed in the paramagnetic ($T > T_C$) and ferromagnetic ($T < T_C$) state. In the first case, the structural state was fixed by quenching from the annealing temperature into water; in the second case, the structural state was obtained by slow cooling. The structural studies of the single-crystal samples were conducted on a four-circle X-ray diffractometer at room temperature. From the X-ray diffraction data, it follows that the alloy, independently on the heat treatment, contains $B2$ clusters, i.e., locally ordered regions with the CsCl-type structure observed in alloys of iron with silicon (to 10 at % Si) and aluminum (7 at % Al) before. In addition to the $B2$-clusters, regions with the $D0_3$ short-range order are observed in the quenched sample; the sizes of these regions significantly increases after annealing in the ferromagnetic state, i.e., a long-range order forms. The relation of the fine structural changes in the alloy due to various heat treatments with its magnetoelastic and magnetostriction properties is discussed.

1. INTRODUCTION

Iron-rich iron−gallium alloys attracted significant scientific interest after A.E. Clark et al. reported in the Conference "Intermag 2000" (Toronto, Canada) for the first time that they detected the increase in the magnetostriction due to addition of gallium in iron by a factor of more than ten, and the maximum was observed at the gallium concentration about 17 at % [1]. In 2003, they reported the results of the measurements of tetragonal magnetostriction coefficient λ_{100} in single-crystal samples of iron−gallium alloys in the dependence on the gallium concentration (4−35 at % Ga) and the conditions of their heat treatment [2]. As is shown in Fig. 1 taken from [2], coefficient λ_{100} increases proportionally to the squared gallium concentration almost to 17 at % Ga and, in this region, it is not dependent on whether the sample was slowly cooled or quenched into water after holding at a temperature of 1000°C. Between 17 and 19 at % Ga, the magnetostriction continues to increase in the quenched samples and begins to decrease in the slowly cooled samples. At the maximum value of $3/2\lambda_{100}$ about 400×10^{-6}, the difference is ~25%.

According to the iron−gallium phase diagram [3], the alloys are in the paramagnetic state and in the $A2$-phase region, or disordered solid solution of gal-

lium in α iron at the gallium concentration about 18 at % and temperatures higher than 750°C. As temperature decreases, they transform into the ferromag-
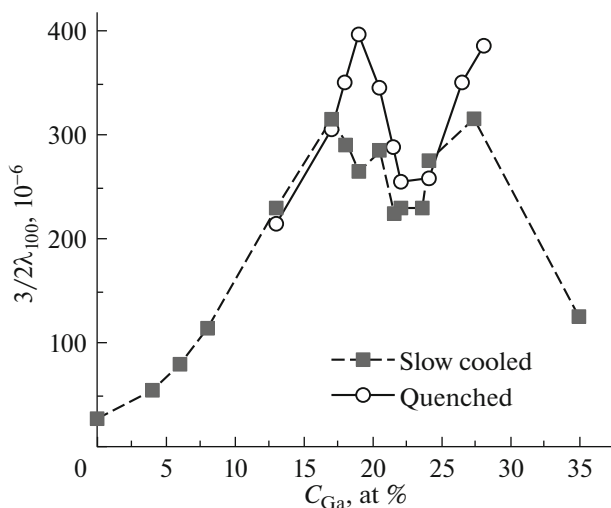
Fig. 1. Dependence of the tetragonal magnetostriction coefficient λ_{100} of the iron−gallium alloy on the gallium concentration C_{Ga} and heat treatment conditions measured in magnetic field $H = 15$ kOe [2].

netic state and to the two-phase region where the *A*2-phase coexists with another phase Fe₃Ga with the *D*0₃-type structure.

The first-principle studies of the chemical ordering in Fe–Ga alloys showed that the transition of the alloy from the paramagnetic to ferromagnetic state is accompanied by a decrease in the effective Ga–Ga interaction energy at the distances of the first and the third neighbors and an increase at the distances of the second neighbors [4]. This result predicts the formation of the *B*2-type structure in the paramagnetic state. The simulation of the alloy structure at 18 at % Ga by the Monte Carlo method in the framework of the same studies showed that, in the ferromagnetic state, the *D*0₃ short-range order must form, in which gallium atoms are the third neighboring atoms.

Since the magnetostriction is an effect determined by the structure, the specific features of gallium atom ordering and a change in the structure as functions of the thermal prehistory play an important role in the giant magnetostriction in the alloy. It was shown using the first-principle calculations [5] that the *B*2 structure is much more promising for an increase in the magnetostriction coefficient with gallium content as compared to *D*0₃. The authors of [6] used the model of randomly oriented pairs of gallium atoms that are the second neighbors and the element of the short-range *B*2 order to explain the effect of the decrease in the magnetic anisotropy in the iron–gallium alloy. They assumed that this is a result of the competition between the crystal anisotropy and the anisotropy of magnetization fluctuations that is due to the local anisotropy of Ga–Ga *B*2 pairs. At the present time, the nature of the giant magnetostriction is still being discussed; however, it is assumed in [6] that namely the existence of such Ga–Ga pairs is the cause of the increase in the magnetostriction, because its value is changed proportionally to the squared gallium concentration in α-FeGa.

The atomistic simulation of the formation of nanostructures in the Fe–19 at % Ga alloy showed [7] that the disordered solid solution of gallium (phase *A*2) can decompose by scheme $A2 \rightarrow B2 \rightarrow D0_3$ with the formation of the *B*2-type nanoregions with sizes from 3 to 10 nm at the intermediate step. However, according to the data of the high-resolution X-ray diffraction for the alloy with 19 at % Ga [8], a short-range order is not observed in the quenched samples, and, in the slowly cooled samples, the regions with the *D*0₃ order occupy approximately one third of the volume and coexist with the disordered *A*2 phase. The X-ray diffraction study of the structure of the slowly cooled single crystals of the Fe₈₁.₆Ga₁₈.₄ and Fe₈₁Ge₉ alloys showed [9] that the short-range order in the arrangement of Ga atoms corresponds to the *D*0₃ type and Ge atoms prefer the chemical ordering of the *B*2 type. Because of this, the authors assumed that it is precisely the *D*0₃

local ordering that is important for the increase in the magneto-elasticity in iron-based metals.

The studies of the local ordering in iron–silicon alloys [10–12] showed that the quenched samples of the alloy with 5–10 at % Si contain clusters with *B*2 ordering. The increase in the silicon concentration from 5–6 at % to 8 at % leads to the formation of small regions with the *D*0₃ order, the sizes and the volume fraction of which increases after 10-min holding at a temperature of 450°C. At 10 at % Si, the *D*0₃ phase consists of regions with long-range order [12]. Figure 2 schematically shows *B*2 clusters; they can be represented as a "core" consisting of two *B*2 cells with a common face surrounded by extended α-Fe cells. The *B*2 clusters have an anisotropic shape; they are more extended along one of the easy-magnetization axes ⟨100⟩. The regions with similar local ordering were observed in single crystals of the Fe–7 at % Al alloy [13].

These results were obtained from the X-ray diffraction data, i.e., after the analysis of the angular distribution of the intensity of a weak but very informative diffuse scattering. At the same time, in order to distinguish the contribution to scattering due to the thermal motion of atoms, the measurements were carried out at low temperatures [14]. The computer simulation of the diffuse scattering confirmed the conclusions obtained from the analysis of the experimental data. The model calculations also allowed one to determine the quantitative relationships in the short-range order atomic structure (the number and the type of atoms, their displacements from the perfect lattice sites) that agree well with the picture of the two-dimensional distribution of the diffuse scattering intensity.

The aim of this study is to use similar approach to elucidate fine specific features of the atomic structure of the iron–gallium alloy subjected to various heat treatments and to connect them with the change in the magnetic properties, the magneto-elasticity, and magnetostriction.

2. EXPERIMENTAL

The X-ray diffraction studies were carried out on single crystals of the Fe–18 at % Ga alloy. The alloy samples were cut from the monolithic crystal grown by the Bridgman method as thin discs (0.3 mm in thickness and 8–9 mm in diameter) with a "Goss" orientation of the crystallographic axes when axes [110] and [001] lie in the disc plane. The samples were subjected to refining vacuum annealing at a temperature of 1050°C for 4 h. The first sample was quenched into room-temperature water (the quenching rate was not less than 400°C/s) after 10-min holding in the paramagnetic state at temperature $T_{an} = 850°C$. It is assumed that a high-temperature holding must lead to disordering gallium atoms in the iron lattice, and the quenching must fix the disordered state. The second
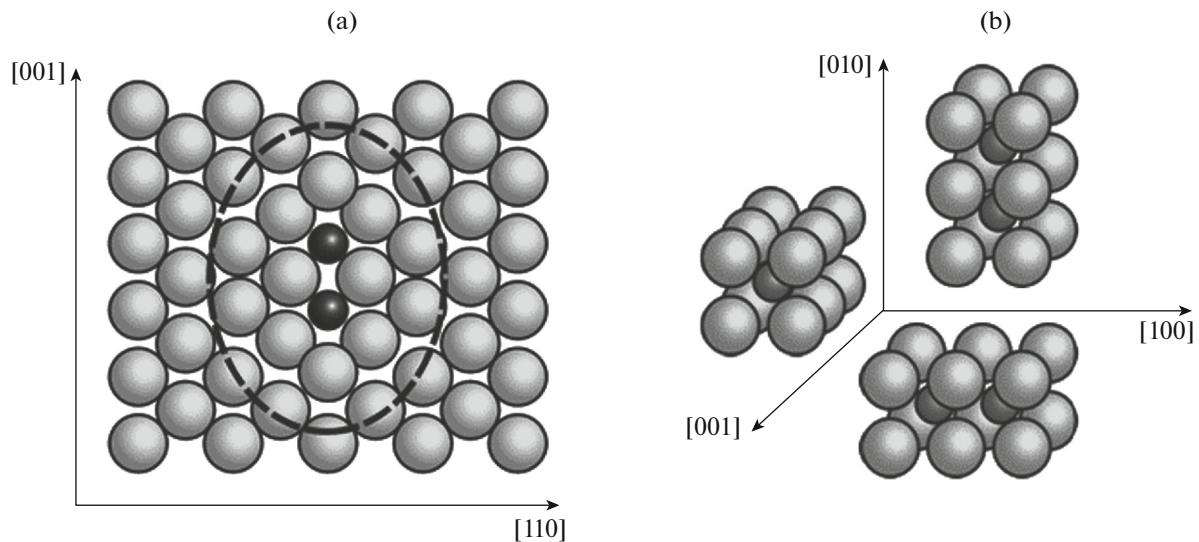
Fig. 2. (a) Schematic representation of the cross section of a $B2$ cluster in plane $(1\bar{1}0)$ and (b) possible orientations of $B2$ clusters along axes $\langle 100 \rangle$.

sample was slowly cooled after 1 h holding in the ferromagnetic state. The annealing temperature ($T_{an} = 450°C$) was much lower than the Curie point of the alloy ($T_C \approx 700°C$), but was sufficient to activate a high diffusion of gallium in iron to quickly attain equilibrium state.

The X-ray diffraction patterns of the alloy samples measured by scanning along different crystallographic directions were compared with analogous scans for an iron single-crystal [13]. This enabled us to reliably separate the contribution from the scattering on the regions with local ordering of impurity Ga atoms and also exclude the contribution of the scattering from diffuse planes and rods caused by thermal motion of atoms which are characteristic for a bcc lattice [14].

The measurements were carried out at room temperature on the four-circle laboratory diffractometer (St. Petersburg Nuclear Physics institute of NRC "Kurchatov Institute") in the transmission geometry. The characteristic radiation of the X-ray tube with a Mo anode ($\lambda = 0.071$ nm) was monochromatized using a pyrolytic graphite crystal. The scattered radiation was registered by an energy-dispersive Si(Li) detector [10], which allows one to significantly improve the signal/background ratio.

3. RESULTS AND DISCUSSION

The bcc-lattice of the α-FeGa alloy, as well as the lattice of pure α-iron, manifest themselves in diffraction as a set of strong narrow peaks with an even sum of indices h, k, l, for example, (110), (200), (211), (220), (310), (400), and so on. The reflections with other combinations of integer indices are forbidden. In the cases of $B2$ or $D0_3$ ordering, the X-ray diffraction patterns of the alloy contain superstructure peaks for which sum $h + k + l$ is an odd number, i.e., peaks with indices (100), (300), (111) and so on. Furthermore, as a result of doubling the cell along the crystallographic axes at the formation of the $D0_3$ phase, the superstructure peaks appear with half-integer indices $h = n/2$, $k = m/2$, and $l = p/2$, where n, m, p are integer odd numbers, for example, (0.5 0.5 0.5), (1.5 0.5 0.5), (1.5 1.5 0.5) (1.5 1.5 1.5), and so on.

At the transition from α-iron to an iron–gallium alloy, as well as in the case of iron-aluminum alloys [13], the main Bragg reflections remain almost unchanged and are only shifted to lower scattering angles because of an increase in the bcc-cell parameter a with increasing gallium concentration [15]. From the angular positions of the peaks, we can obtain the lattice parameters $a = 0.2901(2)$ nm for the first sample and $a = 0.2896(2)$ nm for the second sample (in α-iron, $a = 0.2866$ nm). The lattice parameters of the alloy samples are 1% larger than the parameter in α-iron, and coincide within two–three standard deviations.

Figure 3 shows in logarithmic scale for the intensity the X-ray diffraction patterns obtained by θ–2θ scanning of the reciprocal space along axes [001], [111], [110], and [221]. The strong bcc reflections (002), (222), (110), and (220) are about four orders of magnitude larger than the diffuse scattering that is of interest for us. The examples of the diffuse scattering are shown in Fig. 3 in the intervals between the direct beam and the Bragg peaks (002), (004), (110), and (220) in the corresponding scans a, b, c, and d.

The broad diffuse peaks are observed in the θ–2θ scans measured along directions [111] and [221]. They appear in the places, where the scan trajectory in the
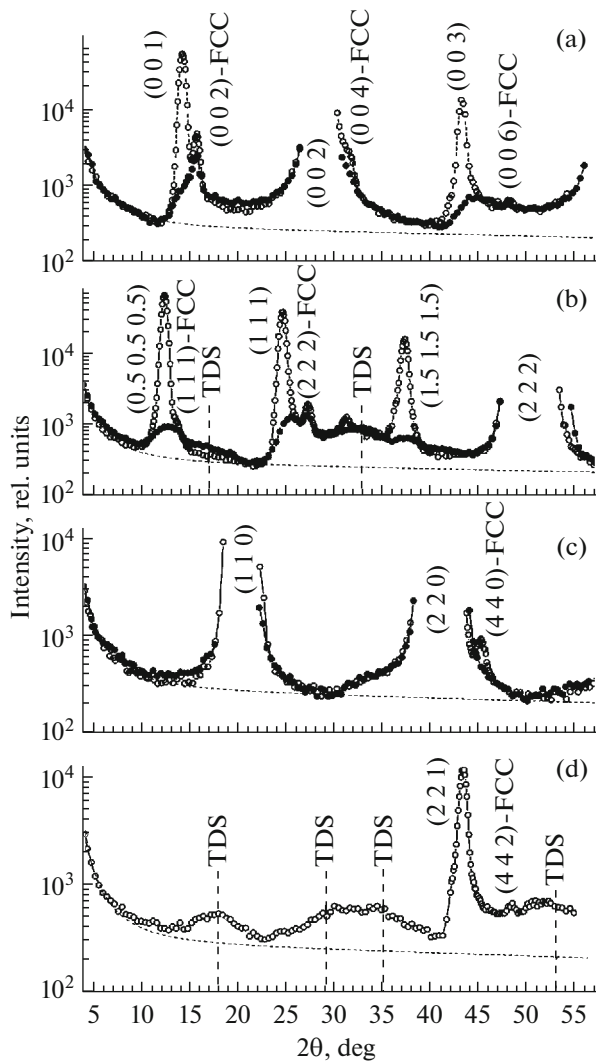
Fig. 3. X-ray diffraction patterns of (full circles) the quenched and (open circles) annealed samples measured during scanning along directions (a) [001], (b) [111], (c) [110], and (d) [221]. The experimental error is approximately equal to the symbol size. The background is the dotted line obtained by the LSM approximation of the experimental points.

reciprocal lattice of the crystal intersects the thermal diffuse scattering (TDS) planes (TDS plane is indicated by vertical dashed lines in Fig. 3). The TDS planes characteristic of crystal with the bcc structure are due to thermal vibrations of atomic chains [111] along themselves [14]. Broad TDS peaks are also observed in similar scans in pure iron single crystals, as we showed before (Fig. 5b, [13]).

The X-ray diffraction patterns of the Fe–Ga alloy sample subjected to annealing in the ferromagnetic state contain significantly more details than the X-ray diffraction patterns of the quenched sample. After the annealing, the narrow superstructure peaks (001) and (003) appear; they are observed in the X-ray diffrac-

tion pattern measured during scanning along axis [001] (Fig. 3a) simultaneously with similar peaks (0.5 0.5 0.5), (111) and (1.5 1.5 1.5) in the diffraction pattern measured when scanning along axis [111] (Fig. 3b). All these peaks appear from quite large regions of the $D0_3$ phase. The narrow peak (221) in the diffraction pattern of the annealed sample measured when scanning along axis [221] has the same origin (Fig. 3d).

The X-ray diffraction patterns shown in Fig. 3 demonstrate, in addition to contributions from the bcc and $D0_3$ phases, the narrow reflections of a new phase denoted as FCC. The peaks of this phase are weak in the diffraction pattern of the quenched sample, but they are seen more clearly in the diffraction patterns of the annealed sample ((hkl)-FCC). From the extinctions and positions of more than ten such peaks, it can be unambiguously stated that the unit cell of this phase is cubic, and its axes coincide with the bcc-cell axes, that it is face-centered cubic (FCC), and its unit cell lattice parameter is ~0.52 nm.

To determine the contributions to scattering from different phases forming in the iron–gallium alloy, the diffraction patterns were described by a set of the peaks whose shapes were given by the Gaussian and Lorentzian functions, and their parameters (position, width, and height) were obtained by the least square method (LSQ) when matching the calculated and the experimental data. Of specific interest is the contribution to scattering from the $B2$ and $D0_3$ phases after quenching and annealing of the alloy samples. This contribution, evidently, is small in the case of the quenched sample, and the contribution from the $B2$ phase in the case of the annealed sample is also small; because of this, to increase the reliability of the LSQ procedure, it is necessary to describe correctly the monotonically decreasing background. For this purpose, from several θ–2θ scans, including [001], [111], and [110], for the annealed sample in the range 5° < 2θ < 55°, we took a whole range 5° < 2θ < 8° and the lowest experimental points at larger angles. A smooth envelope that is the sum of the inclined straight line and the Lorentzian function with a maximum at 2θ = 0 was built through these points using the LSQ procedure. The result is shown by the dashed line in Fig. 3. Further, the background parameters were not varied in processing the diffraction patterns.

The narrow superstructure peaks (001), (003), (111), (0.5 0.5 0.5), (1.5 1.5 1.5), and (221) in the diffraction patterns of the sample annealed in the ferromagnetic state are due to the long-range $D0_3$ ordering. The intensities of even the strongest of them are two orders of magnitude lower than those of bcc peaks. Some of them, such as: (001), (111), (0.5 0.5 0.5), and (1.5 1.5 1.5) are observed as broad diffuse peaks in the diffraction patterns of the quenched sample (Fig. 3).

Figure 4 shows the result of decomposition of the diffraction patterns measured in direction [001] from
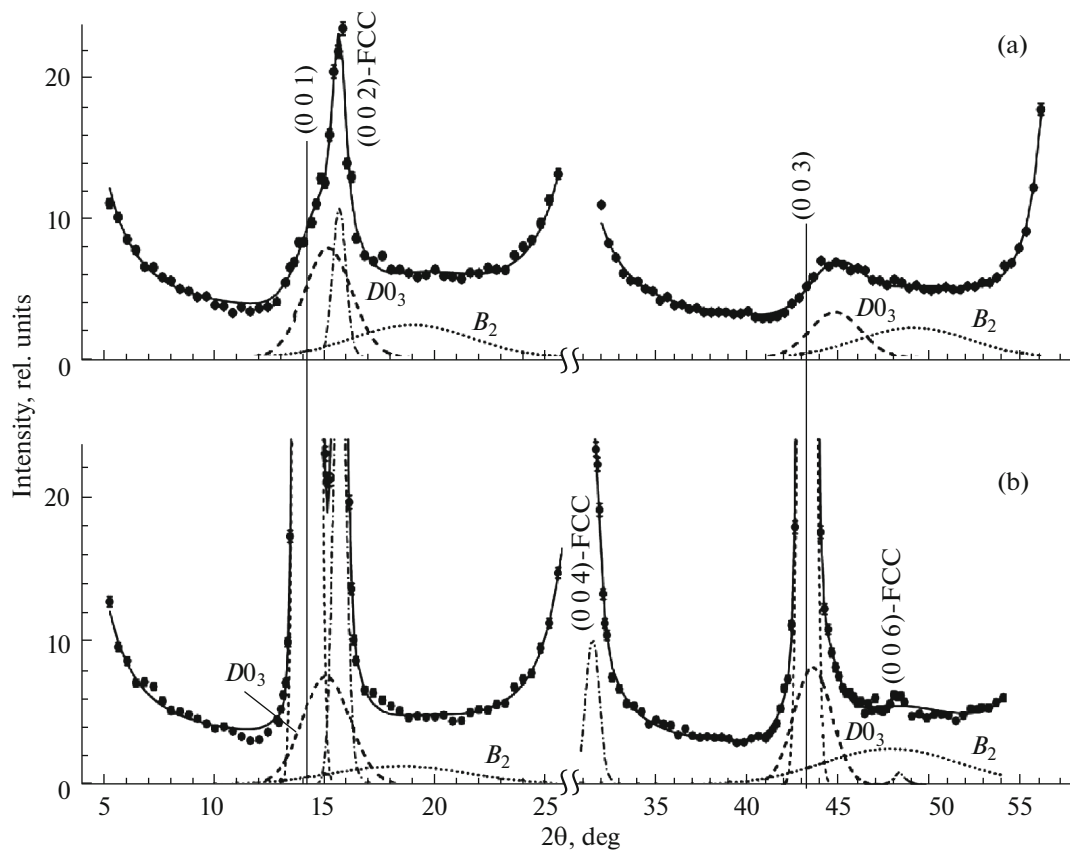
Fig. 4. Angular distribution of the scattering intensity of (a) quenched and (b) annealed alloy samples measured by scanning along axis [001]. The contributions of scattering on the $B2$ clusters, regions with the $D0_3$ ordering, and regions with FCC phase are shown by various lines as separate peaks.

the quenched and annealed samples. As in the case of describing the background, the slopes of the strong bcc peaks (002), (004), and also (222) in the scan along axis [111] were described by the "wing" of the Lorentzian function whose parameters were varied. In each of the diffraction patterns in Fig. 4, the summary curve envelopes the experimental points, contributions from $B2$ and $D0_3$ phase and peaks (002), (004), and (006) of the FCC phase. These decompositions do not allow obtaining quantitative characteristics of the phases, but give their qualitative estimation and clarify the tendency of their changes. The width of the strong $D0_3$ peaks in the diffraction pattern of the annealed sample is about 0.7°, but it is significantly broader for the diffuse $B2$ and $D0_3$ peaks of the quenched sample (~7° and ~3°, respectively). The FCC peaks are narrow (width ~0.9°), which indicates large sizes of this phase regions, but, judging on their intensities, their volume fraction is small. After annealing the sample in the ferromagnetic state, the peaks from the $B2$ phase are changed insignificantly, and narrow and intense (001) and (003) peaks appear in the calculated position for the $D0_3$ phase with a long-range order. However, their asymmetry clearly

observed at the right "wing" of (003) (Fig. 4b) makes us to preserve, in the diffraction pattern decomposition, diffuse $D0_3$ peaks very similar to the peaks separated in the diffraction pattern from the quenched sample (Fig. 4a). It seems likely, the small $D0_3$ clusters that are unambiguously determined in the quenched sample, remain in part after annealing. In this case, it is necessary to note an important fact: unlike the Fe−7 at % Al [13] and Fe−(5−6) at % Si) [10, 11] alloys, in the diffraction patterns of the Fe−Ga alloy studied in this work, the $B2$ peaks are shifted to larger, not to smaller, scattering angles from the calculated positions for (001) and (003) indicated by the vertical lines in Fig. 4.

The mean size of the ordered region (cluster) can be estimated from the peak width using the Scherrer formula [16]. It is ~0.6−0.7 nm, i.e., about the length of two bcc unit cells, for the $B2$-phase clusters in both samples. The regions with the $D0_3$ ordering in the alloy sample quenched after annealing in the paramagnetic state have a size of ~1.6 nm which is the length of two−three $D0_3$ unit cells, and the size increases to ~20 nm in the sample annealed in the ferromagnetic state. The changes in the atomic structure of the iron-gallium
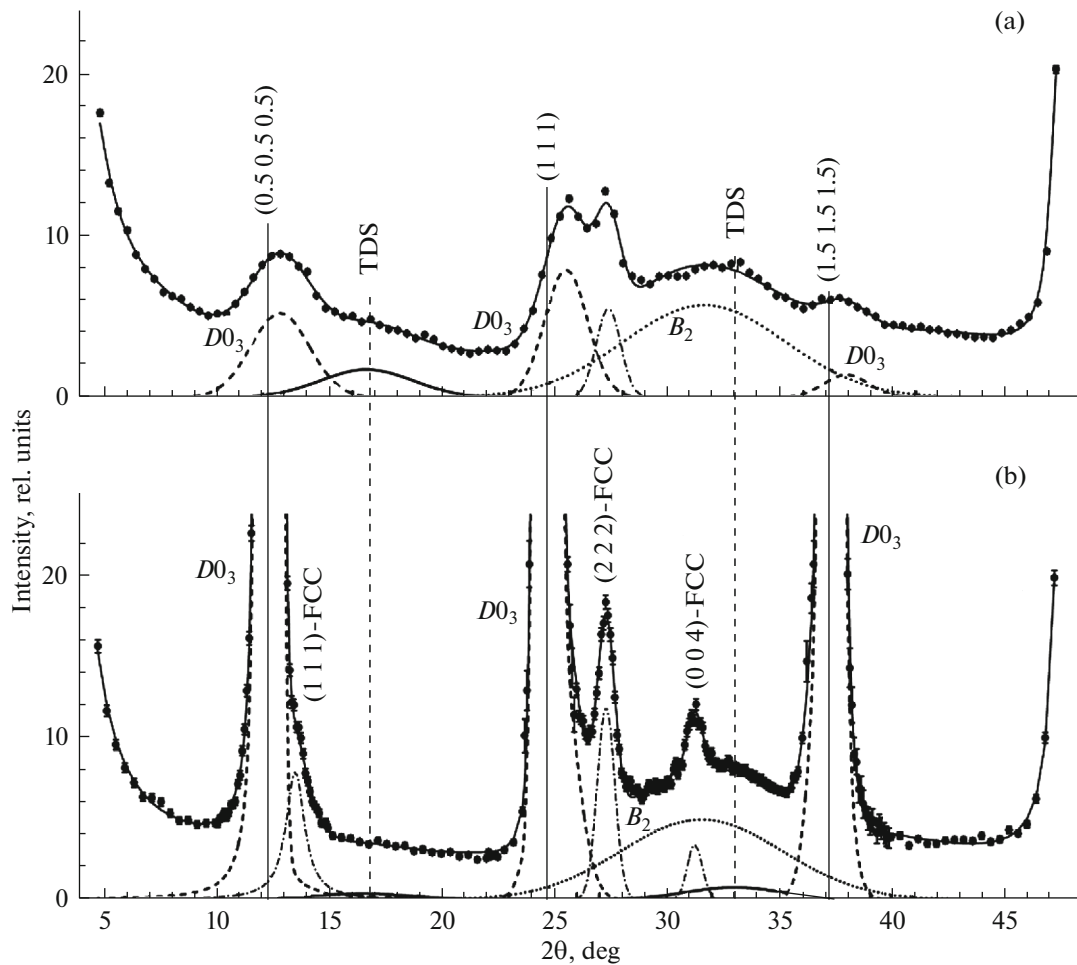
Fig. 5. The same as in Fig. 4 measured by scanning along axis [111]. The contributions of scattering on the $B2$ clusters, regions with the $D0_3$ ordering, and regions with FCC phase are shown by various lines as separate peaks.

alloy agree with the predicted tendencies in the formation of the short-range order during annealing in the dependence on the magnetic state [4].

The diffraction patterns for direction [111] were decomposed by analogy with that how it was made for the diffraction patterns obtained upon scanning along axis [001] (Fig. 4) using the LSQ method. Figure 5 shows the result of this decomposition. It should be noted that, in the case of the quenched sample, all the diffuse $D0_3$ peaks (0.5 0.5 0.5), (111), and (1.5 1.5 1.5) shown in Fig. 5a are shifted to larger scattering angles from the calculated positions indicated by the solid vertical lines exactly as well as peaks (001) and (003) in Fig. 4a. Therefore, the lattice parameter of small $D0_3$ clusters formed in the alloy in the paramagnetic state is smaller than the $D0_3$ unit cell parameter in large $D0_3$-phase regions.

A noticeable decrease in the diffuse scattering intensity shown in Fig. 3 is observed after annealing in the ferromagnetic state in the scan along axis [111] at segments $5° < 2\theta < 10°$ and $14° < 2\theta < 20°$ and in the

scan along axis [001] at segment $17° < 2\theta < 23°$. In the case of the annealed sample, the $D0_3$ peaks obtained during ω scanning, i.e., perpendicularly to direction of the θ–2θ scans are narrow as peak (111) in Fig. 6a, but the diffuse scattering has a larger extent for both the samples. Figure 6b shows, as an example, the ω-scan perpendicularly to axis [001] at $2\theta = 20.4°$ for the quenched sample; it is seen that the intensity is not changed over entire range of the measurements. From this observation, it can be assumed that the decrease in the contribution of the diffuse scattering after annealing is related to the redistribution of Ga atoms between the $A2$ phase, where Ga atoms are single, and phases $D0_3$ and FCC, in which a long-range order forms and, likely, with insignificant increase in the number of the $B2$ clusters.

After annealing, the diffuse scattering intensity in the range $10° < 2\theta < 18°$ when scanning along axis [110] slightly increases, as it is shown in Fig. 3c. At the same time, the (440)-FCC peak forms at an angle $2\theta \sim 45°$. In the Fe–Ga alloy, as well as in the case of
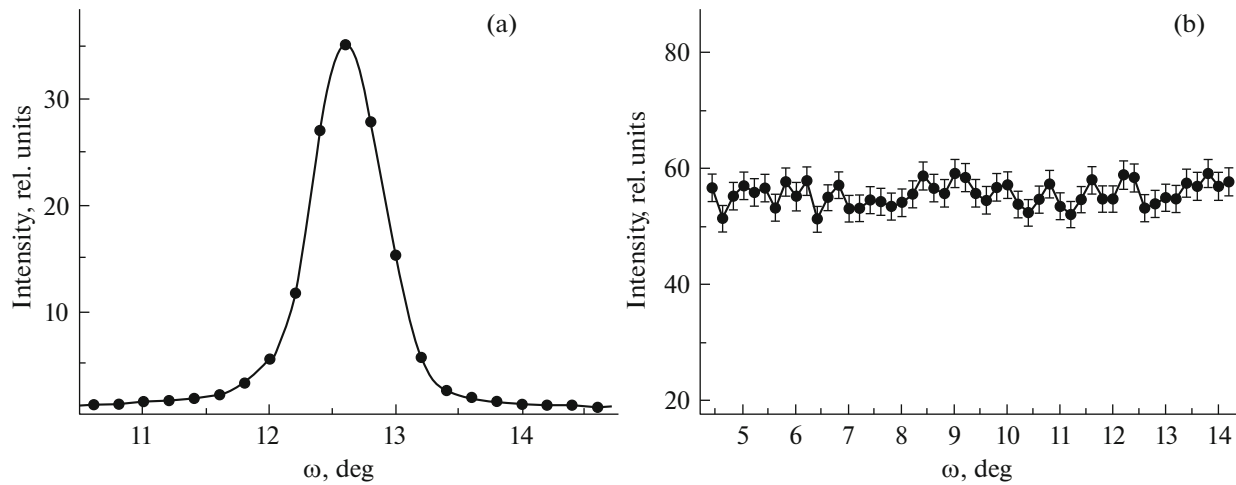
Fig. 6. (a) ω-scans of peak (111) at $2\theta = 25.2°$ for the annealed sample and (b) the scattering background at $2\theta = 20.4°$ for the quenched sample.

Fe−Si [10−12] and Fe−Al [13] alloys, there are not any peculiarities, except for some asymmetry of the background near the (220) peak, as compared to similar scan for the iron single crystal. Most likely, this asymmetry in the form of an elevation of the left "wing" of peak (220) in the range $2\theta \sim 35°$ is due to the contribution of the diffuse scattering.

Before discussing the obtained results, we note an important circumstance once again. The existence of the superstructure peaks of the diffuse scattering (hkl) with an odd sum $h + k + l$ in the diffraction patterns of the alloy is an indicator of a short-range ordering of $B2$-type impurity atoms. The widths of these peaks at half-height shows that their sizes are not larger than the length of two bcc unit cell of the alloy. The shifts of their maxima from the calculated positions to larger scattering angles demonstrates that the bcc unit cells composing a $B2$ cluster are deformed substantially. The shifts of the superstructure peaks from the $B2$ phase were also observed in both iron−silicon [10, 11] and iron−aluminum [13] alloys before, but then the peak maxima were shifted to smaller angles. It was shown that the observed peculiarities of the diffuse scattering are explained by the existence in the alloy of clusters that predominantly consist of two bcc unit cells that are centered by silicon (or aluminum) atoms and have a common face, as is shown in Fig. 2.

The results obtained from the LSQ decomposition of the diffraction patterns can be briefly summed up as follows. In the diffraction patterns of the quenched sample, $D0_3$ peaks (001), (003), (0.5 0.5 0.5), (111), and (1.5 1.5 1.5) are much weaker and broader than those in the annealed sample. Figures 4, 5 depict that the peaks are shifted from their calculated positions in the diffraction patterns to larger scattering angles. In the reciprocal lattice, the shift along axis [001] is $\Delta l \approx 0.05$ and along axis [111] $\Delta h = \Delta k = \Delta l \approx 0.05$. There-fore, the $D0_3$ unit cell parameter is almost 5% smaller than the doubled lattice parameter of the bcc unit cell of the alloy and is ~0.55 nm. In the quenched sample, the mean size of the $D0_3$ phase regions is estimated to be 1.6 nm; i.e., it is equal to the length of three $D0_3$ unit cells.

The diffraction patterns of both the samples have broad diffuse peaks disposed near the (001), (003), and (111) positions. They are shifted from the calculated positions to larger scattering angles in the diffraction patterns by $\Delta l \approx 0.25$ along axis [001] and $\Delta h = \Delta k = \Delta l \approx 0.25$ along axis [111] in the reciprocal lattice indices. Since Δh, Δk, and Δl are approximately the same, it can be assumed that these superstructure reflections from ordered $B2$-phase regions, more correctly, from $B2$ clusters in which local ordering is accompanied by the lattice deformations. The estimation of the $B2$-cluster mean sizes gives ~0.6 nm; therefore, the cluster predominantly consists of two unit cells of the bcc lattice. This fact enables us to assume that the $B2$ clusters in the Fe−Ga alloy have the same nature as the clusters observed before in iron-rich Fe−Si and Fe−Al alloys and shown in Fig. 2 [10, 11, 13].

To determine the structure of the $B2$ clusters in the iron−gallium alloy, we carried out the simulation calculations using the DISCUS program package [17]. First, we simulated the bcc-lattice of the crystal containing the deformed clusters, i.e., pairs of the bcc unit cells having a common face and centered by Ga atoms, by analogy to the calculations in our studies of iron−silicon [10, 11] and iron−aluminum [13] soft magnetic alloys. The cluster deformation was given by the displacements of atoms composing the cluster symmetrical with respect to axis ⟨100⟩ going vertically through Ga atom centers, as shown in Fig. 7. Then, the distribution of the diffuse scattering intensity in planes
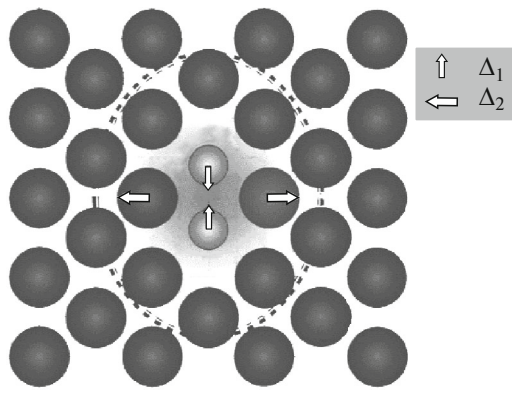
Fig. 7. Scheme of deformations in the nearest environment of Ga atom pair in plane $(1\bar{1}0)$. Gallium atoms are shown by smaller circles and iron atoms by larger circles. The arrows show the directions of displacements of atoms Δ_1 and Δ_2.

(010) and $(1\bar{1}0)$ was calculated for the model of a "crystal" containing a great number of atoms.

In a first step, undeformed $B2$ clusters were randomly distributed in the volume consisting of $32 \times 32 \times 32 = 32768$ bcc unit cells. When fulfilling the condition that a gallium atom has no gallium atoms in the first coordination sphere and can have only one gallium atom in the second sphere, the Ga atom concentration in the model volume becomes to be ~6 at %. Then gallium atoms in the cluster and the nearest iron atoms were displaced from their ideal positions in the lattice, as shown in Fig. 7. By choosing the value of the displacements, we obtained the distribution of the diffuse scattering intensity in planes (010) and $(1\bar{1}0)$ of the reciprocal space that to the best degree corresponds to the experimental peculiarities of the diffuse scattering from the $B2$ clusters or to broad shifted

peaks (001) and (003) separated in Fig. 4 and (111) separated in Fig. 5.

The scattering pattern shown in Fig. 8 was obtained for the relative displacements of the Ga−Ga pair atoms by $\Delta_1 = 0.01$ and the relative displacements of iron atoms disposed in a plane perpendicular to the pair axis and passing through the middle of the distance between them by $\Delta_2 = 0.02$. The directions of the atom displacements Δ_1 and Δ_2 are indicated by the arrows in Fig. 7. The pattern cross section along axis k at the left and the right panels of Fig. 8 correspond to the experimental scan along axis [001] and reproduces diffuse peaks (001) and (003) shifted in the direction of larger scattering angles. This section is shown in Fig. 9, where, for comparison, the contribution of the scattering by deformed $B2$ clusters obtained from the decomposition of the $\theta-2\theta$ scan along axis [001].

The pattern cross section along the abscissa axis in the right part of Fig. 8 and along the diagonals in the left part corresponds to the experimental scan along [110] and reproduces the background asymmetry of peaks (110) and (220) in the experimental diffraction patterns. It is shown in Fig. 10 for two variants of atom displacements Δ_1 and Δ_2, where the variant with $\Delta_2 = 2\%$ is more adequate than the variant with $\Delta_2 = 0$. It is understood that the model of local ordering of Ga atom pairs, i.e., the model of the $B2$ clusters, is simplified and cannot describe well all the peculiarities observed experimentally; moreover, the alloy structure is complex, but even such model describes the main details of the diffuse scattering observed in the experiment.

As for the FCC phase, its influence on the magnetic properties of the alloy is almost improbable, since, judging on the intensities of the corresponding peaks in the diffraction patterns, its volume fraction in
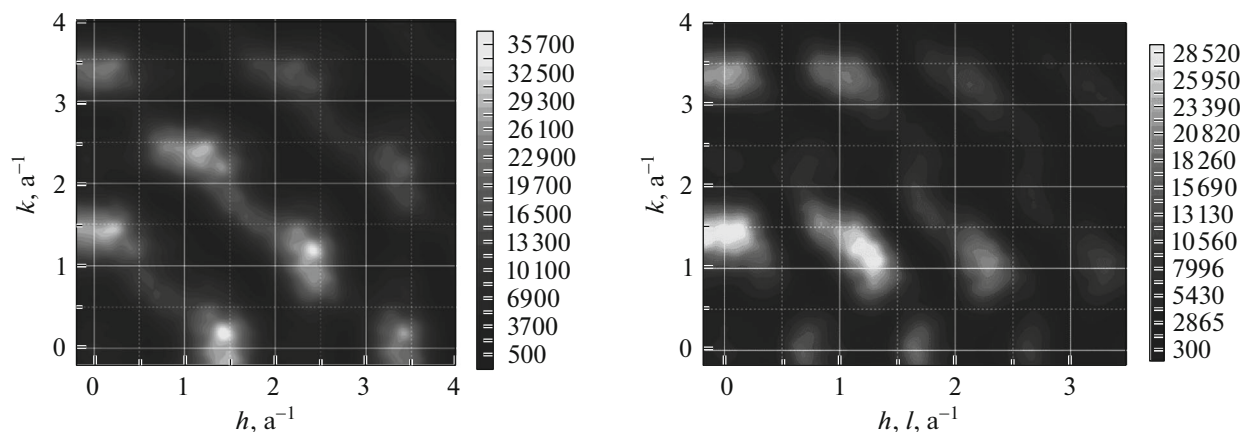
Fig. 8. Distribution of the diffuse scattering intensity in (on the left) plane (010) and (on the right) plane $(1\bar{1}0)$. The calculation was performed for the model structure with random distributions of gallium atom pairs ($B2$ clusters) with the deformations of the local environment shown in Fig. 7.
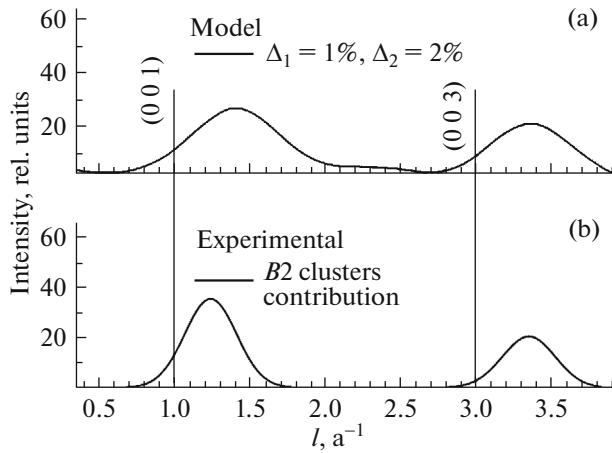
Fig. 9. (a) Model calculation and (b) contribution of the diffuse scattering from $B2$ clusters obtained from the decomposition of the $\theta-2\theta$ scan along axis [001].

Fig. 10. (a) Two variants of the model calculations of the diffuse scattering along axis [110] with different displacement of atoms in a $B2$ cluster and (b) the corresponding scan of the alloy sample subjected to quenching into water.

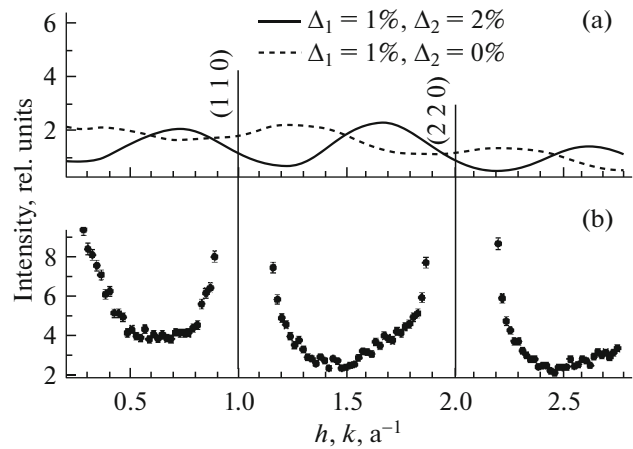the alloy is insignificant both after quenching and after annealing.

Thus, in the case of annealing in the ferromagnetic state, the atomic ordering in the Fe−18 at % Ga alloy mainly occurs with the formation of the $D0_3$ phase and the conservation or insignificant change of the $B2$ clusters. Assuming that, after annealing in the ferromagnetic state, all the sample volume is divided between two phases, namely, $D0_3$ regions and $B2$ clusters, we can estimate the relative fractions of these phases in the sample. The chemical composition in the $D0_3$-phase regions corresponds to the Fe_3Ga formula or to 25 at % of the impurity atoms in the bcc iron. The mean Ga concentration in the regions occupied by $B2$ clusters is approximately 6 at %. The other phase fractions are neglected. Then, the relative fractions of the $D0_3$ phase δ_{D03} and the $B2$ phase δ_{B2} in the alloy are related by equations

$$\delta_{D03}C_{D03} + \delta_{B2}C_{B2} = C_{Ga},$$
$$\delta_{D03} + \delta_{B2} = 1,$$

where $C_{D03} = 0.25$ and $C_{B2} = 0.06$ are gallium concentrations in the $D0_3$-phase regions and in $B2$-cluster regions, respectively, and C_{Ga} is the mean Ga concentration in the alloy. Then,

$$\delta_{B2} = (C_{D03} - C_{Ga})/(C_{D03} - C_{B2}).$$

The substitution of the concentrations gives $\delta_{D03} \approx 0.63$ and the maximum estimation $\delta_{B2} \approx 0.37$, i.e., about 40% of the alloy volume can be occupied by the regions with $B2$ clusters and about 60% by the $D0_3$-phase regions. If, at the mean Ga concentration of 18 at %, all Ga atoms enter into only one $D0_3$ phase, it maximum fraction is ~70% of the sample volume. It is clear that not all Ga atoms enter only into the $D0_3$

phase and the $B2$ clusters. The $A2$-phase regions and even pure-iron regions can exist, but the contribution from them to the diffraction patterns is summed to the strong peaks from the bcc lattice of the alloy.

4. CONCLUSIONS

The X-ray diffraction studies of the atomic structures of the single crystals of the iron−gallium alloys with the gallium content about 18 at % showed that gallium atoms are ordered in the alloy samples. The type of atomic ordering in the crystal regions and the size of the regions are dependent on the heat treatment conditions of the alloy. The diffraction patterns of the sample quenched into water after holding in the paramagnetic state, in addition to strong peaks from the main bcc structure, contain the contribution of the diffuse scattering from the phases $B2$, $D0_3$, and FCC. The annealing in the ferromagnetic state does not lead to a noticeable change in the contribution to the scattering from small (subnanodimenshional, ~0.6 nm) $B2$-phase clusters, while the $D0_3$ and FCC peaks become narrow, their intensities increase (by almost two orders of magnitude for the $D0_3$ peaks). The FCC phase is defined as the cubic face-centered phase. The FCC unit cell axes coincide with the axes of the alloy bcc lattice. The influence of the FCC phase on the magnetic properties is unlikely, since its volume fraction is insignificant.

In [5], it was assumed that there are the peculiarities of the iron−gallium alloy structure that determine the magnetoelastic properties; i.e., the magnetostriction decreases as the $D0_3$-phase volume fraction increases. We observed exactly this fact. In the quenched sample, the $D0_3$-phase volume fraction (the regions with a size of 1.6 nm or as the length of three

unit $D0_3$ cells) is small, but the annealing in the ferromagnetic state leads to the formation of the long-range $D0_3$ order. After quenching, the tetragonal magnetostriction coefficient $3/2\lambda_{100}$ has the maximum value of about 400×10^{-6} (Fig. 1). The $D0_3$-phase regions are significantly increase in volume and the degree of ordering after annealing in the ferromagnetic state. The maximum volume fraction of the $D0_3$-phase regions at the Ga concentration of 18% can be ~70%. When including the presence of $B2$ clusters, the relative volume fractions can be about 60% and 40% for the $D0_3$-phase and $B2$-cluster regions, respectively. Assuming that the $D0_3$ phase negatively influences the magnetoelastic properties of the material, we can understand the difference to 25% in the values of the tetragonal magnetostriction coefficients in the quenched and in slowly cooled samples of the alloy with 19 at % Ga.

The $B2$-phase clusters (pairs of impurity atoms, the second neighbors in the iron bcc lattice) are likely to exist in the alloys with lower gallium concentrations independent of the heat treatment conditions. Since the probability to form such a pair is proportional to the squared concentration of gallium atoms C_{Ga}, the number of the Ga–Ga pairs must be proportional to C_{Ga}^2 if there is tendency to their formation. Thus, it is likely that the existence of the $B2$ clusters and their positive influence on the increase in the magnetostriction determine a quadratic increase in coefficient λ_{100} as C_{Ga} increases from 0 to 17 at %.

Our calculations reproduce the main peculiarities observed in the diffraction patterns even using a strongly simplified model of a $B2$ cluster of anisotropic shape in which gallium and iron atoms are shifted from the ideal lattice sites as shown in Fig. 7. In particular, such peculiarities are: significant shift of the superstructure $B2$ peaks with an odd sum of indices h, k, l from the calculated position to larger scattering angles, and also the background asymmetry near bcc peaks (110) and (220).

The results of the studies agree with the results of the first-principle calculations [4], where the processes of formation of the short-range order in the Fe–Ga solid solutions were considered. It was shown that the interatomic interaction is dependent on the magnetic state of the matrix. When going to the ferromagnetic state, the effective energy of interaction of the Ga–Ga pair, as compared to the paramagnetic state, decreases by a factor of almost two in the case of the first neighbors, increases for the second neighbors, and becomes minimal for the third neighbors. Thus, the short-range $B2$ order preferably forms in the paramagnetic state ($T > T_C$), and the atomic short-range $D0_3$ order corresponds to the equilibrium state of the alloy in the ferromagnetic state ($T < T_C$).

It can be assumed that the mechanism acting in Fe–Ga alloys is similar to that proposed in [18], where a change in the atomic ordering in iron-rich Fe–Si alloy was considered. The $B2$ pairs of the second neighbors of Si atoms (Fig. 2) forming in the paramagnetic state are retained on cooling due to that they form a stable complex with a vacancy preventing the pair dissociation by diffusion. Then, in Fe–Ga alloy too, for the local $D0_3$-type order to occur during annealing in the ferromagnetic state, additional activation of the diffusion process, i.e., overcoming energy barrier of 0.3–0.5 eV is necessary. Thus, the transformation of the $B2$ and $D0_3$ short-range orders does not occur spontaneously as temperature decreases below the Curie point and develops gradually during a long-term annealing at $T < T_C$. Most likely, the volume fraction of the $D0_3$ phase at high gallium concentration from 17 to 20 at % increases as a result of diffusion in it of gallium atoms from the disordered $A2$ phase.

ACKNOWLEDGMENTS

REFERENCES

1. J. R. Cullen, A. E. Clark, M. Wun-Fogle, J. B. Restor, and T. A. Lograsso, J. Magn. Magn. Mater. **226–230**, 948 (2001). doi 10.1016/S0304-8853(00)00612-0

2. A. E. Clark, K. B. Hathaway, M. Wun-Fogle, J. B. Restorff, T. A. Lograsso, V. M. Keppens, G. Petculescu, and R. A. Taylor, J. Appl. Phys. **93**, 8621 (2003). doi 10.1063/1.1540130

3. O. Ikeda, R. Kainuma, I. Ohnuma, K. Fukamichi, and K. Ishida, J. Alloys Compd. **347**, 198 (2002). doi 10.1016/S0925-8388(02)00791-0

4. M. V. Petrik, O. I. Gorbatov, and Yu. N. Gornostyrev, JETP Lett. **98**, 809 (2013). doi 10.7868/S0370274X13240107

5. R. Wu, J. Appl. Phys. **91**, 7358 (2002). doi 10.1063/1.1450791

6. J. Cullen, P. Zhao, and M. Wuttig, J. Appl. Phys. **101**, 123922 (2007). doi 10.1063/1.2749471

7. J. Boisse, H. Zapolsky, and A. G. Khachaturyan, Acta Mater. **59**, 2656 (2011). doi 10.1016/j.Actamat.2011.01.002

8. T. A. Lograsso and E. M. Summers, Mater. Sci. Eng. A **416**, 240 (2006). doi 10.1016/j.msea.2005.10.035

9. M. Huang and T. A. Lograsso, Appl. Phys. Lett. **95**, 171907 (2009). doi 10.1063/1.3254249

10. Yu. P. Chernenkov, N. V. Ershov, V. A. Lukshina, V. I. Fedorov, and B. K. Sokolov, Phys. B (Amsterdam, Neth.) **396**, 220 (2007). doi 10.1016/j.physb.2007.04.008

11. N. V. Ershov, Yu. P. Chernenkov, V. A. Lukshina, and V. I. Fedorov, Phys. Solid State **51**, 441 (2009). doi 10.1134/S1063783409030019

12. N. V. Ershov, Yu. P. Chernenkov, V. A. Lukshina, and V. I. Fedorov, Phys. Solid State **54**, 1935 (2012). doi 10.1134/S1063783412090107

13. N. V. Ershov, Yu. P. Chernenkov, V. A. Lukshina, and O. P. Smirnov, Phys. Solid State **60**, 1661 (2018).

14. Yu. P. Chernenkov, V. I. Fedorov, V. A. Lukshina, B. K. Sokolov, and N. V. Ershov, Phys. Met. Metallogr. **100**, 235 (2005).

15. C. J. Quinn, P. J. Grundy, and N. J. Mellors, J. Magn. Magn. Mater. **361**, 74 (2014). doi 10.1016/j.JMMM.2014.02.004

16. B. D. Cullity and S. R. Stock, *Elements of X-Ray Diffraction* (Prentice-Hall, New York, 2001).

17. Th. Proffen and R. B. Neder, J. Appl. Crystallogr. **30**, 171 (1997). doi 10.1107/S002188989600934X

18. O. I. Gorbatov, A. R. Kuznetsov, Yu. N. Gornostyrev, A. V. Ruban, N. V. Ershov, V. A. Lukshina, Yu. P. Chernenkov, and V. I. Fedorov, J. Exp. Theor. Phys. **112**, 848 (2011). doi 10.1134/S1063776111040066

Translated by Yu. Ryzhkov